Al-Rafidain J Med Sci. 2023;5:247-256.
DOI: https://doi.org/10.54133/ajms.v5i.280

AJMS
Online ISSN (2789-3219)

Research Article

Osseointegration and Histological Picture of Titanium Silicon Gallium Alloy *vs*. Titanium Silicon Alloy and Pure Titanium

Mustafa Sameer Al-Shaikhli[1]*, Hikmat Jameel Abdul-Baqi[1]

[1] *Department of prosthodontics, College of Dentistry, University of Baghdad, Baghdad, Iraq*

Received: 28 August 2023; Revised: 30 September 2023; Accepted: 2 October 2023

Abstract

Background: Using titanium alloy with gallium and silicon could speed up the process of osseointegration, which would mean that titanium-silicon-gallium alloy could be used in more therapeutic situations. ***Objective***: To evaluate the osseointegration and histological features of a newly fabricated Ti-Si-Ga alloy implant. ***Methods***: Samples were fabricated utilizing the powder metallurgy technique. The titanium matrix was augmented with alloying components. The composite materials were produced by the compaction process at a pressure of 900 MPa, followed by sintering at a temperature of 800°C. For the in vivo test, ninety cylindrical specimens (3x6 mm in diameter and height, respectively) were prepared by using a wire-cut machine to cut the mentioned measurements from a sintered cylinder (15 mm in diameter and 6 mm in height) (6 cylinders for each group). ***Results***: The Ti-Si-Ga group showed the highest bone formation area and higher push-out values than the commercially pure Ti and Ti-Si groups in this study. ***Conclusion***: The use of gallium as an alloying element improved osseointegration.

Keywords: Gallium, Osseointegration, Implant, Biomaterial, Alloy

الاندماج العظمي والصورة النسيجية لسبائك التيتانيوم والسيليكون الغاليوم مقابل سبائك السيليكون التيتانيوم والتيتانيوم النقي

الخلاصة

الخلفية: يمكن أن يؤدي استخدام سبائك التيتانيوم مع الغاليوم والسيليكون إلى تسريع عملية الاندماج العظمي، مما يعني أنه يمكن استخدام سبائك التيتانيوم والسيليكون والغاليوم في المزيد من الحالات العلاجية. **الهدف**: تقييم التكامل العظمي والسمات النسيجية لزرع سبيكة Ti-Si-Ga المصنعة حديثا. **الطريقة**: تم تصنيع العينات باستخدام تقنية تعدين المساحيق. تم تعزيز مصفوفة التيتانيوم بمكونات صناعة السبائك. تم إنتاج المواد المركبة من خلال عملية الضغط عند ضغط 900 ميجا باسكال، تليها التلبيد عند درجة حرارة 800 درجة مئوية. بالنسبة للاختبار في الجسم الحي، تم تحضير تسعين عينة أسطوانية (قطرها وارتفاعها 3 × 6 مم ، على التوالي) باستخدام آلة قطع الأسلاك لقطع القياسات المذكورة من أسطوانة ملبدة (قطرها 15 مم وارتفاعها 6 مم) (6 أسطوانات لكل مجموعة). **النتائج**: أظهرت مجموعة Ti-Si-Ga أعلى مساحة تكوين عظمي وقيم دفع أعلى من مجموعات Ti و Ti-Si النقية تجاريا في هذه الدراسة. **الأستنتاج**: أدى استخدام الغاليوم كعنصر صناعة السبائك إلى تحسين الاندماج العظمي.

* ***Corresponding author***: Mustafa S. Al-Shaikhli, Department of prosthodontics, College of Dentistry, University of Baghdad, Baghdad, Iraq; Email: mustafa.Jamil1908@codental.uobaghdad.edu.iq

Article citation: Al-Shaikhli MS, Abdul-Baqi HJ. Osseointegration and histological picture of titanium silicon gallium alloy *vs*. titanium silicon alloy and pure titanium. *Al-Rafidain J Med Sci*. 2023;5:247-256. doi: https://doi.org/10.54133/ajms.v5i.280

INTRODUCTION

Over the last decade, implantology has seen significant advancements, becoming an integral aspect of traditional dentistry. This field has played a pivotal role in enhancing the overall well-being of several patient populations. There has been a lot of research and development into implants because there are more people who need them. This has led to fast technological progress, big changes in implant design, materials, and parts, and easier treatment delivery at all stages [1]. Factors relating to a material's mechanical properties, chemical properties, and biocompatibility all play a role in the selection of dental implants. Regardless of the particular function and application of dental implants, it is crucial that the materials used exhibit excellent resistance to corrosion, biocompatibility, and the absence of any detrimental chemicals [2]. Peri-implantitis is identified as the prevailing etiological factor contributing to the failure of titanium implants in the medium and long term. Peri-implantitis is a pathological disease that manifests in the peri-implant tissues, marked by inflammation in the peri-implant mucosa and consequent gradual degradation of the underlying bone structure [3]. Furthermore, there are other issues that may arise, including fractures, titanium allergy, and corrosion [4–7]. Titanium has the capacity to produce alloys with other elements, which may be used to modify its characteristics. This includes enhancing its strength, performance at high temperatures, resistance to deformation under constant stress, ability to be welded, and malleability [8]. The element Si has been included in many commercial alloys as a means to enhance the resistance of Ti to creep and oxidation when exposed to high temperatures [9]. The potential substitution of Ti-6Al-4V alloy with Ti-Si alloys in the area of implant materials has been investigated, mostly owing to the superior biocompatibility of Si and its comparably low toxicity when compared to other alloy elements such as Al, Cr, V, Ni, and others [10–14]. Gallium (Ga) is an element that exhibits several biological functions, including immunosuppressive qualities, tumor imaging capabilities, anticancer activity, antibacterial effects, anti-inflammatory effects, and prevention of osteoclastogenesis [15]. It has been shown that Ga ions have the capability to substitute iron (Fe) in Fe-dependent redox processes that occur during DNA synthesis in bacteria, ultimately leading to the demise of the bacterial cells [16]. Furthermore, gallium (Ga) has been shown to accelerate the proliferation of osteoblasts, suppress bone resorption, stimulate collagen production, and enhance the creation of bone tissue [17–19]. The aforementioned properties render Ga a suitable therapeutic agent for dental implant modifications aimed at improving osseointegration and augmenting its antibacterial efficiency. The primary objective of this study is to investigate the impact of gallium (Ga) additions on the osseointegration of Ti-Si alloys and pure titanium by preparing Ga-containing Ti alloys.

METHODS

Alloys synthesis and processing

The metals used as initial substances for the synthesis of the alloys in this investigation consisted of titanium powder with a purity of 98.5% (Fluka, Switzerland), silicon powder with a purity of 95% (Merck, Germany), and gallium metal with a purity of 99.5% (Thomas Baker Chemicals, India). The average particle size of pure titanium powder was determined to be less than or equal to 6.5755 micrometers, whereas the average particle size of silicon powder was discovered to be less than or equal to 2.457 micrometers. The weights that have been predetermined to be used in the study are: 1) 70% Ti + 30% Si; 2) 70% Ti + 15% Si + 15% Ga; and 3) 100% Ti. The sample preparation procedure commenced with the determination of the necessary material quantities based on specified ratios. Subsequently, titanium (Ti) powders were combined with gallium (Ga) metal, and the resulting mixture was subjected to titration. This involved placing the mixture in a plastic container within an amalgamator, which was operated at a speed of 4,800 revolutions per minute (rpm) for a duration of 90 seconds. Following this step, the container was transferred to a heat-preserving box and maintained at a temperature of approximately 32°C for a period of 24 hours. On the subsequent day, the predetermined amount of silicon (Si) powder was added to the container. In the case of Ti-Si samples, the mixture of the pre-weighed powders underwent titration exclusively. The powders were mixed for a duration of 10 minutes using a ceramic grinder manufactured by CAPCO in the United Kingdom, with a rotational speed set at 110 revolutions per minute (rpm). Following this procedure, the mixture was prepared for compaction and pressing. A locally fabricated metal mold was used for the purposes of this investigation. The mold used in this study was constructed using a rigid steel material. It had four distinct components, namely the die, base, punch, and ejector base (Figure 1). The die used in the experiment was a hollow, cylindrical die made of hardened steel. It had a height of 75 mm, an inner diameter of 15 mm, and an exterior diameter of 26 mm. The base consisted of a stainless-steel disc measuring 13 mm in height and 21 mm in diameter. Positioned in the center of the base was a short, solid rod with dimensions of 14.95 mm in height and 6 mm in diameter. This rod was put into the canal of the die when placed on the base. The punch used in the experiment was constructed using a solid rod of hardened steel with the following dimensions: a height of 114 mm and a diameter of 14.95 mm. The aforementioned punch was used in the process of compacting alloy powder inside a die, as well as facilitating the ejection of the resulting specimen from

said die. In order to generate a cylindrical sample with a diameter of 15 mm, the height of which is determined by the weight of the added mixture, it was observed that samples with a thickness of 6 mm were generated using 4 grams of the mixture. The weighted quantity was put into the die using a glass funnel. Graphene powder from Shaanxi Greenyo Biotech in China was used as a lubricant due to its ability to simplify the insertion and withdrawal of the punch. The punch was introduced into the die, and afterwards, the mould was positioned onto the tray of the hydraulic press manufactured by MEGA in Spain (Figure 1).

Figure 1: (Left) Mold used in the study (A: The punch, B: The die, C: The base, D: the ejector base) (Middle) hydraulic press (MEGA, Spain) (Right) sample preparation using wire-cut machine.

A pressure of 900 MPa was deemed appropriate for the compression process, accompanied by a holding duration of 6 minutes. The specimens underwent a sintering process within a vacuum furnace, utilizing a quartz tube, and in an argon environment. Step sintering was employed, involving three distinct temperature stages: 250°C with a holding time of 30 minutes, 500°C with a holding time of 30 minutes, and finally 800°C with a holding time of 240 minutes. The heating and cooling rate was set at 10°C/min. Subsequently, the specimens were left within the furnace, maintaining an inert atmosphere, while being cooled to room temperature. While for titanium samples, the sintering cycle was 1000 °C for 3 hours at 10°C/min heating and coaling rate [20]. The sintered composites underwent a grinding process using silicon carbide (SiC) paper, beginning with a gradual progression from 800 to 2000 grit while being cooled with a flow of water. Subsequently, the composites were subjected to ultrasonic cleaning using a 99.5% acetone bath (specifically, Bio-wash from Bio Art) for a duration of 15 minutes. Following this, the finished samples were washed with 99.9% ethanol and subsequently dried in an electric oven at a temperature of 120°C for a duration of 10 minutes, as described in [21].

Implant samples preparation

Ninety cylindrical specimens were prepared (3x6 mm diameter and height, respectively) by using a wire-cut machine to cut the mentioned measurements from a sintered cylinder (15 mm x 6 mm) (10 cylinders for each group), as shown in Figure 1. The sintered cylinders were categorized into 3 groups: the first group was commercially pure Ti; the second group was 70% Ti–30% Si; and the final group was 70% Ti–15% Si–15% Ga. Then each group was subdivided into two other subgroups for two intervals of implant time, one for two weeks and the other for a six-week interval. Five samples from each subgroup were used for histological and histomorphometrical studies, while the other 10 samples were used for a push-out test to measure the adherence force of bone to implant. All samples were finished, polished, and ultrasonically cleaned by the acetone path, then washed with ethanol and dried as mentioned previously. The specimens were sterilized using a double vacuum autoclave (22) Class B, which began the operation with three cycles of vacuum and then pressure, which continued for about 48 minutes, after which sterilization began at a temperature of 134.5°C for 3.5 minutes, followed by drying for 15 minutes until the time of the procedure.

Determination of microstructural phases

X-ray diffraction (XRD) was used to evaluate the microstructural phases present in the Ti-Si and Ti-Si-Ga alloys. The phases of the sintered samples were analyzed using an automated X-ray diffractometer in combination with Cu-K radiation ($\lambda = 1.5406$ Å). The experiment was conducted with a current of 40 milliamperes (mA) and a voltage of 40 kilovolts (kV). The diffraction patterns were recorded at the laboratory's ambient temperature, with a 10-second interval between each angular step. Each angular step corresponds to an increment of 0.02 degrees. The process of peak indexing was conducted following the guidelines set out by the Joint Committee on Powder Diffraction Standards (JCPDS) of the International Centre for Diffraction Data.

Animals study design

The animal study was approved by the Research Ethics Committee of the College of Dentistry/University of Baghdad according to the ethical acceptance of project no. 740222 on 1/12/2022. Thirty healthy adult white male New Zealand rabbits weighing about 2.5 kg and aged 10–12 months were employed as experimental animals. The rabbits were housed in private animal houses in special animal cages for at least two weeks before surgical operation in the same standard environment in the cages where they could freely access clean water and were fed a mixture of standard pellets, fresh vegetables, and green grass [23]. The procedures

were carried out at the Al-Dyhaa Center for Agricultural and Veterinary Services, Al-Jadreah, Baghdad. The experimental rabbits were separated into two major groups (2 and 6 weeks) based on the healing interval, with each main group consisting of fifteen animals. Five animals were euthanized for histology examination, while the remaining ten were sacrificed for mechanical testing via a push-out bond strength test. Two implants were placed in the proximal third of the lateral side of the femoral bone: the hole close to the femur head received an implant made of 70% Ti-30% Si as well as another implant made of 70% Ti-15% Si-15% Ga about 1.0 cm from the first hole. The left femur bone received one hole for the titanium control group. The implantation procedure was carried out in both femurs, from the mesial bone side to the distal bone side.

Surgical procedure

Using scalpel no. 23, we made a 3cm incision into the skin and subcutaneous tissue. A hole 3 mm wide and around 5 mm deep was created with a handpiece bur for dental implants utilizing an angled surgical handpiece (1:5) (800 rpm), and torque was 35 N. cm installed on a prosthetic engine and profuse saline irrigation coolant. One hole was drilled into the control group's left femur bone for the CP Ti implants. The right side received two holes, with the hole closest to the femur head receiving the 70% Ti-30% Si implant test group and the second hole receiving the 70% Ti-15% Si-15% Ga implant test group approximately one centimeter away. There was around 1mm of the implant protruding from the bone when the specimens were carefully tapped into the holes. Both the control and experimental implants were placed in separate plastic bags and autoclaved for 50 minutes at 134 degrees Celsius. After that, a 2/0 absorbable suture was used to sew the muscles and fascia, and a 3/0 silk suture was used to stitch the skin.

Euthanization of the animals

Each healing interval ended with the subcutaneous administration of 2 ml of ketamine at a dosage of 20 mg/ml/kg BW to sacrifice the rabbits from each group. Left and right femurs with implant specimens were exposed, and all the flesh was removed with a diamond disc mounted on a surgical handpiece. The implanted regions were divided into tiny block samples. The fifteen rabbits were separated into ten rabbits for the push-out test and five rabbits for the histological analysis.

Push out test

The anesthetic solutions, equipment, and materials used in the implantation technique were also used in this step. Ten rabbits were euthanized on the same day for a push-out failure test using a universal testing machine with a 2000 N load at a rate of 1 mm/min and a 3 mm-diameter working head. According to the manufacturer's instructions, powder and liquid self-curing acrylic resin had been mixed. To facilitate the push-out test, the femur was imbedded in a dough mixture of self-curing acrylic resin at the bone's base and on its sides. The acrylic block had been left to cure at ambient temperature. A hole was made at the acrylic base with bone below the implanted specimen at least 3.5 mm in diameter to record the pure shear force required between the implant and bone, as shown in [24]. The highest failure load was measured in Newton (N), and the shear stress was calculated by dividing the applied force by the circumferential area of the cylindrical implant specimen, which served as the contact area. The circumference of the implant had increased in proportion to its height.

Histological study

A prosthetic engine with a straight hand piece (strong 90, Korea) used a disc cutter to incise the bone surrounding the implant while using regular saline for irrigation. The bone-implant block was acquired by a cutting procedure performed about 0.5 cm from the screw of the implant. The blocks underwent fixation by being immersed in a 10% formalin solution for a minimum duration of three days. Following the completion of slide preparation, a light microscope (Pro.Way, China) was used to capture photos of the sections at magnifications of 4, 10, and 40.

Histomorphometric analysis

Histomorphometric findings were examined by means of a light microscope. The photos were taken with a Canon 6DMkII camera by using the AmScope microscope adapter for a Canon DSLR. Calibration was first done using a microscope calibration slide and software application (ImageJ) [25]. For measuring the new bone formation area (NBFA), images at magnification 10X were opened using the ImageJ application, then the free hand selection tool was used to outline the required area, followed by selecting measure from the Analyze drop-down menu (or pressing command-m on mac) to get the measurement. Two (10X) pictures were taken for each side of the slide, as it was not possible to include all the new bone formation area in one (10X) image. The area measured by both images was added to calculate the NBFA.

Statistical analysis

The suitable statistical methods were used in order to analyze and assess the results using GraphPad PRISM version 9. The descriptive statistics include a summary statistic of the reading distribution (mean, SD, minimum, and maximum) and a bar chart for graphical

presentation. Shapiro-Wilk test to test the normality of the distribution of quantitative variables among groups. T-test to find the difference in the mean between two groups. The analysis of variance (ANOVA) method was used to assess the equality of means. In the process of making comparisons, a p-value of less than 0.05 was considered statistically significant. The Tukey post hoc test was used in this research to explore differences between multiple group means.

RESULTS

The XRD patterns of the control Ti-Si specimen are demonstrated in Figure 2A. The strongest peaks pattern at 28.6754, 39.9986, and 47.4220 correspond with the intensity counts 1519, 258, and 197, respectively. The data were indexed according to the Powder Diffraction Files (PDF) for Ti5Si4 (JCPDS-ICDD file # 27-0907), α-TiSi2 (JCPDS-ICDD file # 35-0785), and TiSi2 (JCPDS-ICDD file # 10-0225). The XRD patterns of the Ti-Si-Ga specimen are demonstrated in Figure 2B.

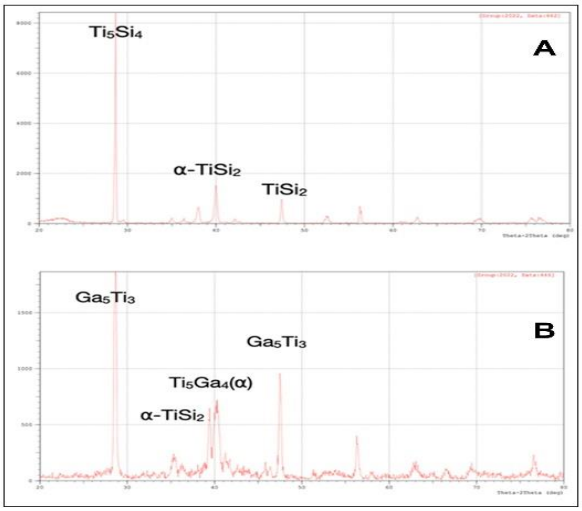

Figure 2: X-Ray Diffraction results (XRD), (A) Ti-Si samples, and (B) Ti-Si-Ga samples.

The strongest peaks pattern at 28.6510, 47.5180, 40.2207, and 39.4372 correspond with the intensity counts 295, 165, 93, and 83, respectively. The data were indexed according to the Powder Diffraction Files (PDF) for Ga5Ti3 (JCPDS-ICDD file # 42-0811), Ga5Ti3 (JCPDS-ICDD file # 42-0811), Ti5Ga4 (JCPDS-ICDD file # 16-0139), and α-TiSi2 (JCPDS-ICDD file # 35-0785). Shear bond strength mean values for different groups of CPTi, Ti-Si, and Ti-Si-Ga implants after 2 and 6 weeks of implantation were summarized in Figure 3.

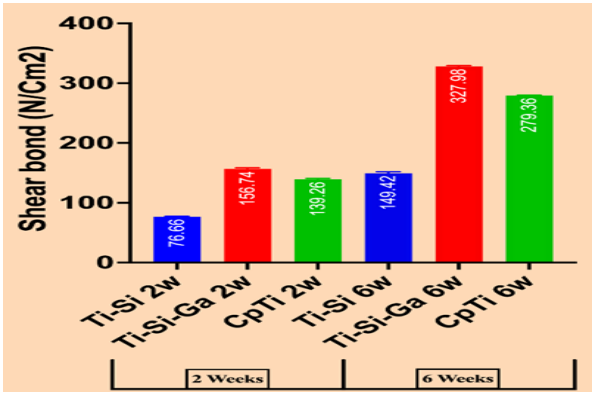

Figure 3: Shear bond strength mean values of all test groups at 2 time intervals (2 weeks and 6 weeks).

In the results of the present study, the shear bond strength mean values at 2 weeks after implantation showed that the Ti-Si-Ga implants had the highest mean value, followed by the CpTi implants, while the Ti-Si implants had the lowest mean value. At 6 weeks after implantation, the results showed that the Ti-Si-Ga implants had the highest mean value, followed by the CpTi implants, while the Ti-Si implants had the lowest mean value. The shear bond strength means values of the test groups (Ti-Si, CpTi, and Ti-Si-Ga) implant had been measured with the paired t-test to show the significant difference between each group after 2 and 6 weeks. As summarized in Table 1, there was a significant increase in the adhesion strength of all groups from the 2- to 6-week healing period.

Table 1: Shear bond (N/cm2) values comparison of each group (Ti-Si, CpTi, and Ti-Si-Ga) at 2 and 6 weeks

Materials	N	Shapiro-Wilk test		Time (wk)	(N/cm^2) mean±SD	*t*-test	*p*
		W	*p*				
Ti-Si-Ga	10	0.9484	0.6491	2	156.7±5.34	102.7	<0.0001
	10	0.9680	0.8714	6	328.0±4.62		
Ti-Si	10	0.9466	0.6285	2	76.66±3.28	22.91	<0.0001
	10	0.8747	0.1132	6	149.4±7.51		
CpTi	10	0.8747	0.1135	2	139.3±4.7	116.6	<0.0001
	10	0.9173	0.3353	6	279.4±2.58		

The shear bond strength comparison among tested groups at each time interval (2, 6 weeks) is shown in Table 2. ANOVA with the post hoc Tukey test showed a highly significant difference between every two tested groups and also revealed a statistically highly significant difference between the CpTi group and Ti-Si-Ga and the CpTi group and Ti-Si and Ti-Si-Ga groups and Ti-Si after 2 and 6 weeks of implantation in rabbits.

Table 2: Shear bond strength comparison among groups (Ti-Si, CpTi, and Ti-Si-Ga) at each interval (2 and 6weeks)

Time	Material	N	mean±SD	*p* (ANOVA)	Tukey's multiple comparisons test	*p*
2 Weeks	Ti-Si-Ga	10	156.7±5.34	F= 867.6 *p*<0.0001	Ti-Si-Ga *vs*. Ti-Si	<0.0001
	Ti-Si	10	76.66±3.28		Ti-Si-Ga *vs*. CpTi	<0.0001
	CpTi	10	139.3±4.70		Ti-Si *vs*. CpTI	<0.0001
6 Weeks	Ti-Si-Ga	10	328.0±4.62	F= 3031 *p*<0.0001	Ti-Si-Ga *vs*. Ti-Si	<0.0001
	Ti-Si	10	149.4±7.51		Ti-Si-Ga *vs*. CpTi	<0.0001
	CpTi	10	279.4±2.58		Ti-Si *vs*. CpTI	<0.0001

After 2 weeks of implantation of pure titanium, the photomicrograph showed implant space surrounded by native bone with the formation of new woven bone at the margin of the native bone, separated by a reversal line (black arrow) (Figure 4 A and B). The new bone formation at the implant side had numerous active bumps. Osteoblasts (OB) were arranged at the periphery of the bone in a row, and there were very few osteoclasts (OCL), while osteocytes (OCT) were embedded in lacunae trabeculae (Figure 4).

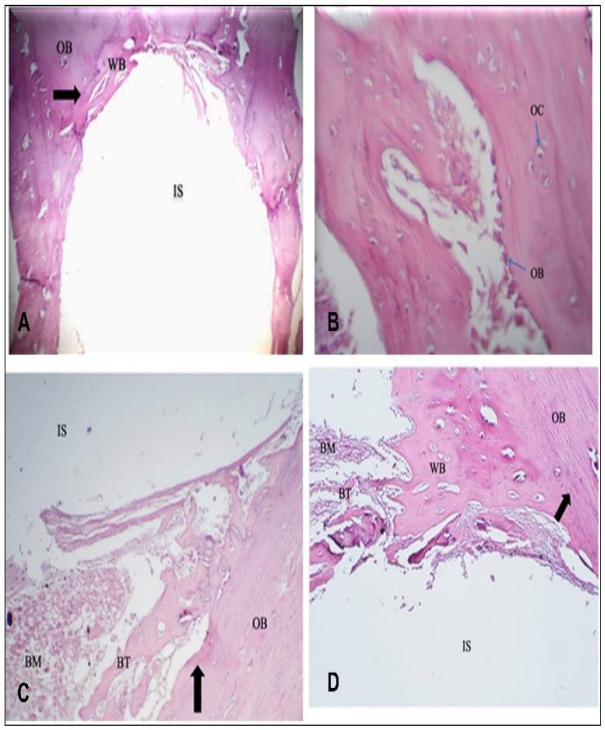

Figure 4: Photomicrograph of H and E stained tissue at 2 weeks, Implant space (IS), Bone marrow (BM), Woven bone (WB), Old bone (OB), Trabecular bone (BT). (A) (4 X) cross section of CpTi; (B) (40X) cross section of CpTi; (C) (10 X) cross section of Ti-Si. (D) (10X) cross section of Ti-Si-Ga.

A similar histological picture was seen in the other groups (Figures 4C and D). The histological feature after 6 weeks demonstrates that all implant specimens reveal the presence of mature bone surrounding the implant with numerous osteons (Haversian system), which manifest with osteocytes embedded in lacunar arranged in a circular pattern around the Haversian canal (central canal) (Figure 5). As shown in Table 3, it compares the new bone formation among groups after a 6-week healing interval. It was noted that the highest new bone area mean value was in the Ti-Si-Ga group, followed by CpTi, and finally, the Ti-Si group was 0.5656 mm^2, 0.4422 mm^2, and 0.2968 mm^2, respectively.

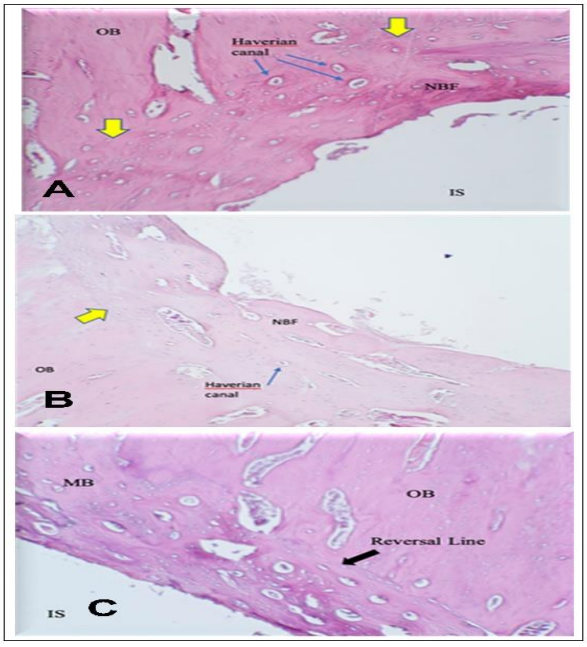

Figure 5: Photomicrograph of H and E stained tissue at 6 weeks Implant space (IS), New Bone Formation (NBF), Old bone (OB), reversal line (yellow and black arrow). A) (10X) cross section of CpTi; B) (10X) cross section of Ti-Si; C) (10X) cross section of Ti-Si-Ga.

Table 3: Comparison of New bone area among groups (CpTi, Ti-Si, and Ti-Si-Ga) at 6 weeks

Time	Material	N	Descriptive statistic (mm^2) mean±SD	*p* ANOVA	Tukey's test	*p*
6 Weeks	Ti-Si-Ga	5	0.566±0.038	F= 39.07 *p*<0.0001	Ti-Si-Ga *vs*. Ti-Si	<0.0001
	Ti-Si	5	0.297±0.060		Ti-Si-Ga *vs*. CpTi	0.0011
	CpTi	5	0.442±0.094		Ti-Si *vs*. CpTI	0.0002

DISCUSSION

Titanium (Ti) and its alloys are extensively used in contemporary medical applications such as bone fixators, artificial joints, dental implants, and several other areas. Since the 1960s, CpTi has been used with success in dental implant procedures, and its biocompatibility with hard tissues is generally acknowledged [26]. It is very important for dental implants to integrate with the bone and soft tissues in the trans-mucosal area and for osseointegration to happen between the bone and implant. This is especially important for people who already have health problems. The typical smooth and bio-inert titanium-based implants have a lower level of STI quality compared to native tissue, namely teeth [27]. The present study design is to enhance the Ti alloy (Ti-Si) biocompatibility and osseointegration through the addition of gallium (Ga) due to multiple studies stating the beneficial effects of Ga, including enhanced osteoblast growth, inhibited bone resorption, promoted collagen synthesis, and improved bone tissue formation [17,18,28]. X-ray diffraction (XRD) patterns of Ti-Si and Ti-Si-Ga after the sintering process showed that the sintering cycle (step sintering was used, the temperatures used were 250 °C holding time for 30 minutes, 500 °C holding time for 30 minutes, and finally 800 °C holding time for 240 minutes at 10°C/min heating and coaling rate, then the specimens were left in the furnace in an inert atmosphere inside the furnace, with flow of argon gas for cooling to the room temperature) was suitable to produce Ti-Si intermetallic compounds Ti5Si4 at 28.67°, α-(TiSi2) at 39.9°, and TiSi2 at 47.422°without unwanted or impurities phases nor pure metal, this result is in agreement with [29]. For Ti-Si-Ga samples, the XRD patterns revealed the formation of the following intermetallic phases: Ga5Ti3 at 28.5°, α (Ti5Ga4) at 40.153°, and Ga5Ti3 at 47.39°. The Ga became highly evident in the α-Ti phase, with little shifting of the α-(TiSi2) peak due to the addition of Ga and the formation of α (Ti5Ga4). All diffractograms show reflections belonging only to the α-phase. This is mainly due to the fact that gallium (Ga) acts as an α-stabilizing solute, leading to an elevation in the allotropic transition temperature of titanium (Ti) from the α phase (hexagonal close-packed) to the β phase (body-centered cubic) upon Ga dissolution in Ti [30]. In this study, the bone implant bond strength of Ti-Si-Ga implant specimens was evaluated and compared with Ti-Si and CpTi implant specimens. The force needed to push the implant specimens out was measured after 2 and 6 weeks of implantation in the rabbit femur. The results indicate that all groups that were tested exhibited a significant enhancement in shear strength after a six-week period in comparison to a two-week duration. The observed outcomes may be attributed to the typical sequential process of bone repair, assuming the use of a biocompatible implanted substance. According to the literature study, it was observed that after a period of two weeks, rabbits exhibited a significant bony defect. This defect was characterized by a substantial presence of marrow tissue containing woven bone, which subsequently underwent replacement by lamellar bone and the formation of freshly developed trabeculae [31–33]. Therefore, this particular bone type exhibits a limited connection with the implanted materials, leading to a diminished capacity to withstand applied loads and an increased susceptibility to bond failure. At the conclusion of the sixth week, there was a notable increase in shear strength as compared to the two-week period, which may be attributed to the development of dense and mature bone formation. This finding is consistent with [34], who posited the notion that the conversion of freshly developed woven bone into a lamellar structure begins throughout the period spanning from day 9 to 6 weeks in rabbits' bone fractures. [35] reported that the development of dense bone, while incomplete, occurs within a six-week timeframe in the radius bone defect of rabbits. The bond failure values were higher for the Ti-Si-Ga group after two and six weeks. Recent research has demonstrated the potential osseointegration effect of Ga ions in increasing numbers. Li et al. (2016) and Wang et al. (2021) discovered that Ga ions stimulate in vitro osteoblast differentiation [36,37]. Gómez-Cerezo et al. (2018) developed a bioactive glass containing Ga and proposed that Ga ions can promote osteogenic differentiation at an early stage [38]. Recently, another in vivo study by Li et al. (2023) showed that the rat intramedullary nail model also demonstrated the superior osseointegration effect of the Ti-Ga alloy [39]. The Ti-Si group has the lowest value of shear bond when compared to the other groups. This may be due to the formation of a Si-rich layer between bone and implant. It is thought that the Si layer

is a vitreous silica-like gel. The Si layer may be a weak zone for bonding between bone and the implant in early-term implantation [40]. At two weeks, the histological image of the tested groups showed new bone formation in the areas adjacent to the implant surfaces, with extensive areas of bone marrow containing woven bone in contact with the implant surface. A Haversian system is formed by the arrangement of osteocytes in a concentric fashion at the six-week mark of bone regeneration and maturation. These findings were consistent with [41,42]. The Ti-Si-Sioup showed mature new bone, but the measured area of bone formation was less than that of the CpTi group and the Ti-Si-Ga group at both time intervals. This may be attributed to the Si-rich layer between bone and implant, as mentioned before being a week point [40]. Also, the silicides are very hard but have brittle phases [43, 44], which are found in the Ti-Si group, as was shown in the XRD test of this group. This brittle phase (silicides) may have caused micro cracks and fractures during the insertion of the implant, which may have affected the implant stability. One of the requirements for successful osseointegration of dental implants is the achievement and maintenance of optimal implant stability [45]. The primary instability of implants with a micromotion greater than 100 to 150 μm has been shown to negatively impact osseointegration [46]. Ti-Si-Ga exhibited bioactive behavior promoting bone formation because the inclusion of Ga compounds has enhanced the effect on the activity of osteoblasts, which play an essential role in bone remodeling [47]. Verron et al. (2012) stated that gallium's effects on bone regeneration can be broken down into four parts: 1) inhibiting expression of genes like the osteocalcin gene and the NFATc1 gene; 2) decreasing the secretion of enzymes like MMP13; 3) disrupting calcium balance through the TRPV-5A channel; and 4) making hydroxyapatite crystallize more and making minerals less soluble [28]. Osteocalcin is a bone matrix protein that only osteoblasts make; it can cause osteoclasts to break down bone [48]. It was found that gallium turned down the expression of the Nfatc1 gene and was important for RANKL-induced osteoclast differentiation. Matrix metalloproteinase (MMP13), also known as collagenase 3, is a major enzyme that breaks down the matrix and resorbs bones. Notably, gallium could stop collagenase-3 from doing its job. TRPV-5A is a calcium channel that is highly expressed in osteoclasts and involved in intracellular calcium homeostasis [28].

Study limitations

The study has a few limitations, such as the difficulty of dealing with a new material that lacks its standard parameters, the fact that push-out mechanical testing is a destructive method, and time constraints.

Conclusion

The results indicated good osteointegration in the Ti-Si-Ga and CpTi control groups, which was better than the Ti-Si group at 6 weeks. Histological pictures revealed that Ti-Si-Ga and Ti-Si have good bone formation that is comparable to the CpTi control group. The Ti-Si-Ga-Si-Ga had good osteointegration and new bone formation in vivo, making these materials promising as dental implants.

Conflicts of interest

There are no conflicts of interest.

Funding source

The authors did not receive any source of fund.

Data sharing statement

Supplementary data can be shared with the corresponding author upon reasonable request.

REFERENCES

1. Qassadi W, Alshehri T, Alshehri A. Review on Dental Implantology. *Egypt J Hosp Med*. 2018;71(1):2217–2225. doi: 10.12816/0045293.
2. Elias CN, Lima JHC, Valiev R, Meyers MA. Biomedical applications of titanium and its alloys. *JOM*. 2008;1;60(3):46–49. doi: 10.1007/s11837-008-0031-1.
3. Berglundh T, Armitage G, Araujo MG, Avila-Ortiz G, Blanco J, Camargo PM, et al. Peri-implant diseases and conditions: Consensus report of workgroup 4 of the 2017 World Workshop on the Classification of Periodontal and Peri-Implant Diseases and Conditions. *J Clin Periodontol*. 2018;45(S20):S286–291. doi: 10.1002/JPER.17-0739.
4. Lee JH, Kim YT, Jeong SN, Kim NH, Lee DW. Incidence and pattern of implant fractures: A long-term follow-up multicenter study. *Clin Implant Dent Relat Res*. 2018;20(4):463–469. doi: 10.1111/cid.12621.
5. Hassan AH, Al-Judy HJ, Fatalla AA. Biomechanical effect of nitrogen plasma treatment of polyetheretherketone dental implant in comparison to commercially pure titanium. *J Res Med Dent Sci*. 2018;6(2):367. doi: 10.5455/jrmds.20186257.
6. Mohammed AA, Hamad TI. Assessment of coating zirconium implant material with nanoparticles of faujasite. *J Baghdad Coll Dent*. 2021;33(4):25–30. doi: 10.26477/jbcd.v33i4.3016.
7. Vijayaraghavan V, Sabane AV, Tejas K. Hypersensitivity to titanium: A less explored Area of research. *J Indian Prosthodont Soc*. 2012;12(4):201–207. doi: 10.1007/s13191-012-0139-4.
8. Lautenschlager EP, Monaghan P. Titanium and titanium alloys as dental materials. *Int Dent J*. 1993;43(3):245–253. PMID: 8406955.
9. Froes FH, (Ed.), Titanium: physical metallurgy, processing, and applications. ASM international; 2015. doi: 10.31399/asm.tb.tpmpa.9781627083188.
10. Kim HS, Kim WY, Lim SH. Microstructure and elastic modulus of Ti–Nb–Si ternary alloys for biomedical

applications. *Scr Mater*. 2006;54(5):887–891. doi: 10.1016/j.scriptamat.2005.11.001.
11. Hsu HC, Wu SC, Hsu SK, Li YC, Ho WF. Structure and mechanical properties of as-cast Ti–Si alloys. *Intermetallics*. 2014;47:11–16. doi: 10.1016/j.intermet.2013.12.004.
12. Hsu HC, Wu SC, Hsu SK, Liao YH, Ho WF. Bioactivity of hybrid micro/nano-textured Ti-5Si surface by acid etching and heat treatment. *Mater Des*. 2016;104:205–210. doi: 10.1016/j.matdes.2016.05.009.
13. Hsu HC, Wu SC, Hsu SK, Liao YH, Ho WF. Effect of different post-treatments on the bioactivity of alkali-treated Ti–5Si alloy. *Biomed Mater Eng*. 2017;28(5):503–514. doi: 10.3233/BME-171693.
14. Saxena V, Kumar V, Rai A, Yadav R, Gupta U, Singh VK, et al. Optimization of the bio-mechanical properties of Ti–8Si–2Mn alloy by 1393B3 bioactive glass reinforcement. *Mater Res Express*. 2019;6(7):075401. doi: 10.1088/2053-1591/ab1280.
15. Qiu C, Lu T, He F, Feng S, Fang X, Zuo F, et al. Influences of gallium substitution on the phase stability, mechanical strength and cellular response of β-tricalcium phosphate bioceramics. *Ceram Int*. 2020;46(10 Part B):16364–6371. doi: 10.1016/j.ceramint.2020.03.195.
16. Stuart BW, Stan GE, Popa AC, Carrington MJ, Zgura I, Necsulescu M, et al. New solutions for combatting implant bacterial infection based on silver nano-dispersed and gallium incorporated phosphate bioactive glass sputtered films: A preliminary study. *Bioact Mater*. 2022;8:325–3240. doi: 10.1016/j.bioactmat.2021.05.055.
17. Verron E, Masson M, Khoshniat S, Duplomb L, Wittrant Y, Baud'huin M, et al. Gallium modulates osteoclastic bone resorption in vitro without affecting osteoblasts. *Br J Pharmacol*. 2010;159(8):1681–1692. doi: 10.1111/j.1476-5381.2010.00665.x.
18. Zhang C, Yang B, Biazik JM, Webster RF, Xie W, Tang J, et al. Gallium nanodroplets are anti-Inflammatory without interfering with iron homeostasis. *ACS Nano*. 2022;16(6):8891–8903. doi: 10.1021/acsnano.1c10981.
19. Verron E, Loubat A, Carle GF, Vignes-Colombeix C, Strazic I, Guicheux J, et al. Molecular effects of gallium on osteoclastic differentiation of mouse and human monocytes. *Biochem Pharmacol*. 2012;83(5):671–679. doi: 10.1016/j.bcp.2011.12.015.
20. Al-Hassani F. Studying the effect of cobalt percentage on the corrosion rate of sintered titanium dental implants. *AIP Conference Proceedings*. 2019;2190(1). doi: 10.1063/1.5138497.
21. Hussain Z, N MI, Bk D. Effect of alloying elements on properties of biodegradable magnesium composite for implant application. *J Powder Metall Min*. 2017;06(03). doi: 10.4172/2168-9806.1000179.
22. El-Wassefy N, El-Fallal A, Taha M. Effect of different sterilization modes on the surface morphology, ion release, and bone reaction of retrieved micro-implants. *Angle Orthod*. 2015;85(1):39–47. doi: 10.2319/012014-56.1.
23. Am A, L T, J I. Studying biomimetic coated niobium as an alternative dental implant material to titanium (in vitro and in vivo study). *Baghdad Sci J*. 2018;15(3):0253–0253. doi: 10.21123/bsj.2018.15.3.0253.
24. Han JM, Hong G, Lin H, Shimizu Y, Wu Y, Zheng G, et al. Biomechanical and histological evaluation of the osseointegration capacity of two types of zirconia implant. *Int J Nanomedicine*. 2016;11:6507–6516. doi: 10.2147/IJN.S119519.
25. Abdullah ZS, Mahmood MS, Abdul-Ameer FMA, Fatalla AA. Effect of commercially pure titanium implant coated with calcium carbonate and nanohydroxyapatite mixture on osseointegration. *J Med Life*. 2023;16(1):52–61. doi: 10.25122/jml-2022-0049.
26. Hanawa T. Titanium–tissue interface reaction and its control with surface treatment. *Front Bioeng Biotechnol*. 2019;7:170. doi: 10.3389/fbioe.2019.00170.
27. Jayasree A, Gómez-Cerezo MN, Verron E, Ivanovski S, Gulati K. Gallium-doped dual micro-nano titanium dental implants towards soft-tissue integration and bactericidal functions. *Mater Today Adv*. 2022;16:100297. doi: 10.1016/j.mtadv.2022.100297.
28. Verron E, Bouler JM, Scimeca JC. Gallium as a potential candidate for treatment of osteoporosis. *Drug Discov Today*. 2012;17(19):1127–1132. doi: 10.1016/j.drudis.2012.06.007.
29. Liu Z, Liu Z, Ji S, Liu Y, Jing Y. Fabrication of Ti-Si intermetallic compound porous membrane using an in-situ reactive sintering process. *Mater Lett*. 2020;271:127786. doi: 10.1016/j.matlet.2020.127786.
30. Antonova NV, Tretyachenko LA. Phase diagram of the Ti–Ga system. *J Alloys Compd*. 2001;317–318:398–405. doi: 10.1016/j.matlet.2020.127786.
31. Matos MA, Araújo FP, Paixão FB. Histomorphometric evaluation of bone healing in rabbit fibular osteotomy model without fixation. *J Orthop Surg*. 2008;3(1):4. doi: 10.1186/1749-799X-3-4.
32. Zhao J, Xiao S, Lu X, Wang J, Weng J. A study on improving mechanical properties of porous HA tissue engineering scaffolds by hot isostatic pressing. *Biomed Mater Bristol Engl*. 2006;1(4):188-192. doi: 10.1088/1748-6041/1/4/002.
33. Ou KL, Hou PJ, Huang BH, Chou HH, Yang TS, Huang CF, et al. Bone healing and regeneration potential in rabbit cortical defects using an innovative bioceramic bone graft substitute. *Appl Sci*. 2020;10(18):6239. doi: 10.3390/app10186239.
34. Zhao Y, Yang S, Wang G. Study of trabecular bone fracture healing in a rabbit model. *Int J Clin Exp Med*. 2018;11(8):7651–765. doi: 10.1161/hq1001.097781.
35. Bigham-Sadegh A, Torkestani HS, Sharifi S, Shirian S. Effects of concurrent use of royal jelly with hydroxyapatite on bone healing in rabbit model: radiological and histopathological evaluation. *Heliyon*. 2020;6(7). doi: 10.1016/j.heliyon.2020.e04547.
36. Li J, Wang GB, Feng X, Zhang J, Fu Q. Effect of gallium nitrate on the expression of osteoprotegerin and receptor activator of nuclear factor-κB ligand in osteoblasts in vivo and in vitro. *Mol Med Rep*. 2016;13(1):769–777. doi: 10.3892/mmr.2015.4588.
37. Wang M, Yang Y, Chi G, Yuan K, Zhou F, Dong L, et al. A 3D printed Ga containing scaffold with both anti-infection and bone homeostasis-regulating properties for the treatment of infected bone defects. *J Mater Chem B*. 2021;9(23):4735–4745. doi: 10.1039/D1TB00387A.
38. Gómez-Cerezo N, Verron E, Montouillout V, Fayon F, Lagadec P, Bouler JM, et al. The response of pre-osteoblasts and osteoclasts to gallium containing mesoporous bioactive glasses. *Acta Biomater*. 2018;76:333–343. doi: 10.1016/j.actbio.2018.06.036.
39. Li F, Wang J, Huang K, Liu Y, Yang Y, Yuan K, et al. Ga-containing Ti alloy with improved osseointegration for bone regeneration: In vitro and in vivo studies. *Compos*

Part B Eng. 2023;256:110643. doi: 10.1016/j.compositesb.2023.110643.
40. Kitsugi T, Nakamura T, Oka M, Yan WQ, Goto T, Shibuya T, et al. Bone bonding behavior of titanium and its alloys when coated with titanium oxide (TiO2) and titanium silicate (Ti5Si3). *J Biomed Mater Res*. 1996;32(2):149-156. doi: 10.1002/(SICI)1097-4636(199610)32:2<149::AID-JBM1>3.0.CO;2-T.
41. Shapiro F. Bone development and its relation to fracture repair. The role of mesenchymal osteoblasts and surface osteoblasts. *Eur Cell Mater*. 2008;15:53-76. doi: 10.22203/ecm.v015a05..
42. Al-Tamemi EI. Analysis of inflammatory cells in osseointegration of CpTi implant radiated by low level laser therapy. *J Baghdad Coll Dent*. 2015;27(1):105–110.
43. Kasraee K, Yousefpour M, Tayebifard SA. Mechanical properties and microstructure of Ti5Si3 based composites prepared by combination of MASHS and SPS in Ti-Si-Ni and Ti-Si-Ni-C systems. *Mater Chem Phys*. 2019;222:286-293. doi: 10.1016/j.matchemphys.2018.10.024.
44. Kasraee K, Yousefpour M, Tayebifard SA. Microstructure and mechanical properties of Ti5Si3 fabricated by spark plasma sintering. *J Alloys Compd*. 2019;779:942–949. doi: 10.1016/j.jallcom.2018.11.319.
45. Javed F, Romanos GE. The role of primary stability for successful immediate loading of dental implants. A literature review. *J Dent*. 2010;38(8):612–620. doi: 10.1016/j.jdent.2010.05.013.
46. Szmukler-Moncler S, Salama H, Reingewirtz Y, Dubruille JH. Timing of loading and effect of micromotion on bone–dental implant interface: review of experimental literature. *J Biomed Mater Res*. 1998;43(2):192–203. doi: 10.1002/(SICI)1097-4636(199822)43:2<192::AID-JBM14>3.0.CO;2-K.
47. Aldrich MB, Rasmussen JC, Fife CE, Shaitelman SF, Sevick-Muraca EM. The development and treatment of lymphatic dysfunction in cancer patients and survivors. *Cancers*. 2020;12(8):2280. doi: 10.3390/cancers12082280.
48. Kim JM, Lin C, Stavre Z, Greenblatt MB, Shim JH. Osteoblast-osteoclast communication and bone homeostasis. *Cells*. 2020;9(9). doi: 10.3390/cells9092073.